Institution of MECHANICAL ENGINEERS

Journal of ENGINEERING IN MEDICINE

Special Issue Article

Development and evaluation of an image-free computer-assisted impingement detection technique for total hip arthroplasty

Tobias Renkawitz[1], Martin Haimerl[2], Lars Dohmen[2], Michael Woerner[1], Hans-Robert Springorum[1], Ernst Sendtner[1], Guido Heers[1], Markus Weber[1] and Joachim Grifka[1]

Abstract

Periprosthetic or bony impingement in total hip arthroplasty (THA) has been correlated to dislocation, increased wear, reduced postoperative functionality with pain and/or decreased range of motion (ROM). We sought to study the accuracy and assess the reliability of measuring bony and periprosthetic impingement on a virtual bone model prior to the implantation of the acetabular cup with the help of image-free navigation technology in an experimental cadaver study. Impingement-free ROM measurements were recorded during minimally invasive, computer-assisted THA on 14 hips of 7 cadaveric donors. Preoperatively and postoperatively the donors were scanned using computed tomography (CT). Impingement-free ROM on three-dimensional CT-based models was then compared with corresponding, intraoperative navigation models. Bony/periprosthetic impingement can be detected with a mean accuracy limit of below 5° for motion angles, which should be reached after THA for activities of daily living with the help of image-free navigation technology.

Background

Total hip arthroplasty (THA) is among the most performed procedures in modern orthopedic surgery worldwide. One of the major problems associated with this demanding surgical procedure is early postoperative instability, dislocation, and implant failure caused by impingement.[1,2] Impingement in THA can be associated with component-to-component contact (periprosthetic impingement), bone-to-bone contact (bony impingement), or component-to-bone contact (bone-to-prosthesis impingement). Previous studies have shown that the risk for impingement may be influenced by the surgical approach, soft tissue tension, and prosthetic design.[2–4] However, the most important cause for impingement in THA is the combined orientation of the cup and stem. The surgeon's intraoperative task is therefore to weigh stable component position against optimal postoperative range of motion (ROM) without any forms of impingement.[2,5] Nowadays, THA is increasingly performed on active patients using less invasive, tissue-preserving techniques and reduced incision lengths.[6] Contemporaneously, it becomes progressively difficult for the orthopedic surgeon to estimate the component position precisely, and since impingement is a dynamic process, it has been difficult to identify on the basis of an intraoperative clinical evaluation.[2,3,7] In this context, computer-assisted orthopedic surgery (CAOS) in THA has the potential to couple three-dimensional simulations with real-time

[1]Department of Orthopaedic Surgery, Regensburg University Medical Center, Bad Abbach, Germany
[2]Brainlab AG, R&D Surgery, Feldkirchen, Germany

Corresponding author:
Tobias Renkawitz, MD Department of Orthopedic Surgery, Regensburg University Medical Center, Asklepios Klinikum Bad Abbach, Kaiser Karl V. Allee 3, 93077 Bad Abbach, Germany.
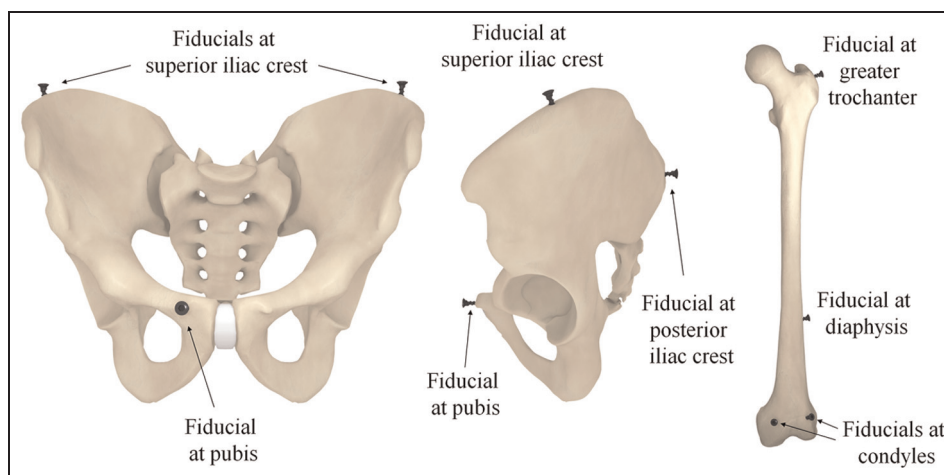Email: t.renkawitz@asklepios.com

Figure 1. Placement of fiducials at the pelvis and femur used to match the intraoperatively acquired navigation data with the CT data sets.
CT: computed tomography.

evaluations of surgical performance, which has brought these developments from the research room all the way to clinical use. Image-free–based navigation systems without the need of additional preoperative or intraoperative image acquisition have stood the test to significantly reduce the variability in positioning the acetabular component and have shown to precisely measure leg length and offset changes during THA.[7,8] So far, image-free navigation technology was not able to implement a comprehensive patient-specific ROM optimization.

Within this study, we have developed an image-free impingement detection method, which simulates and thereby detects bony and prosthetic impingement intraoperatively. The purpose of the current study was to study the accuracy and assess the reliability of measuring bony/periprosthetic impingement on a virtual three-dimensional model with the help of image-free navigation technology in an experimental cadaver study. In particular, we asked whether our approach achieves accurate results for ROM values that are crucial to perform activities of daily living after THA.

Methods

Seven cadaveric donors (three females and four males) were provided by the Institute of Anatomy, Medical University of Graz, Graz, Austria; all were embalmed with Thiel's fixation method that allows a natural tissue feeling and joint movement during surgery.[9] The mean body mass index of the donors was 26.7 kg/m^2 (range, 21.5–37.2 kg/m^2).

Preoperatively, all donors were positioned on a solid spine board (Spencer Rock spine board; Spencer, Parma, Italy) in supine position. Screws were inserted percutaneously through stab incisions as fiducial landmarks at the superior and posterior iliac crests, pubic tubercles, greater trochanters, femoral diaphysis, and

into the femoral condyles (Figure 1). Then, the whole donor including the spine board was wrapped and secured with broad cling film and scanned by computed tomography (CT) (Somatom Sensation 16; Siemens, Erlangen, Germany).

Surgical procedure

Fourteen minimally invasive, computer-assisted THAs using the anterolateral single-incision Micro-Hip® (DePuy, Warsaw, IN, USA) approach were performed in a lateral decubitus position as usual; the main goal was to implant the acetabular and femoral components in a stable position. Press-fit acetabular components, cement-free hydroxyapatite-coated stems, and metal/ceramic heads (Pinnacle, Corail; DePuy, Warsaw, IN, USA) were used. Navigation was performed with the help of an image-free navigation system (Prototype Hip 6.0; Brainlab Navigation System, Feldkirchen, Germany). For the navigation process, reference pins (two Kirschner wires of 3.2 mm diameter) were inserted into the anterior iliac crest and into the ventrolateral third of the distal femur after stab incisions were made. Dynamic reference bases were then attached to the pins. As a next step, the anterior superior iliac spine (ASIS) and pubic tubercle points were registered using a reference pointer positioned on the skin surface. These points define the reference coordinate system of the pelvis, that is, anterior pelvic plane (APP) and midsagittal plane as the symmetry plane of both ASIS points. On the femoral side, the medial and lateral aspects of the epicondyles and ankle points were registered. These points defined the center of the condyles as well as ankles. The knee was held in a 90° flexed position during the acquisition of the ankle points. After osteotomy of the femoral neck and removal of the head, the femur was exposed. Points at the femoral resection plane were
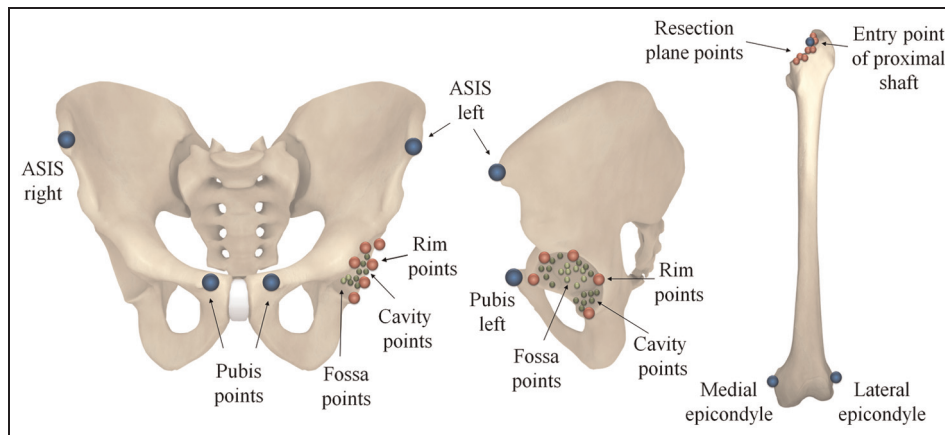
Figure 2. Intraoperatively acquired landmarks for the generation of a virtual individual three-dimensional bone model. Points that were directly acquired on the femoral or pelvic bone are illustrated. Reconstructed points (i.e. center of rotation) or points on the ankles are omitted.

ASIS: anterior superior iliac spine.

registered. Reaming of the femoral medullary canal incorporated various navigated registration/measurement steps of the femoral anatomy, including the entry point of the proximal shaft and the stem antetorsion. Then, the acetabular anatomy including fossa, cavity, and rim was registered and reamed. The center of rotation of the hip joint was determined by matching a sphere into the points acquired in the acetabular cavity. All landmarks and verification information were logged by the navigation system for further analysis. Figure 2 illustrates the acquired landmarks that were later used for generating an individual three-dimensional model of the donor's anatomy. After the insertion of the acetabular cup, its final position was verified, that is, recorded by the navigation system. The uncemented femoral component was placed, followed by a measurement (verification) of the position of the implant. Finally, the head was placed on the femoral component, the joint repositioned, and the layers closed.

Creation of patient-specific three-dimensional bone models

A multistage bone morphing technique that combines affine point matching via an iterative closest point (ICP) technique,[10] point distribution models (active shape models),[11] and spline-based nonrigid deformations[12] was used to fit the individual three-dimensional virtual model to the acquired landmarks. Implant information was added based on the position of the implants as given by the verification steps. The geometry of the implants was based upon three-dimensional computer-aided design (CAD) models that were provided by the implant manufacturer (DePuy, Warsaw, IN, USA) and integrated into the implant database of the navigation software. All implant components (i.e. cup, liner, head, and stem) were included in the models. Cup orientation was set to a standard orientation of 45° radiographic inclination and

15° radiographic anteversion.[13] The resulting three-dimensional models represented the postoperative situation including bony and prosthetic structures.

For the CT-based analysis, the femora and pelvis were segmented manually in each of the preoperative CT data sets using image processing software (iPlan Hip prototype; Brainlab, Feldkirchen, Germany). This resulted in three-dimensional CT models that were compared with the corresponding models generated from the intraoperatively acquired landmark data (intraoperative/image-free models). For this purpose, the CT models were aligned with the image-free models using the fiducial landmarks. This resulted in a registration between the CT and intraoperative models. This registration was used to transfer the surgical information, that is, femoral resection plane, implant position, and orientation into the preoperative CT scans. Based on this information, the implant geometry was integrated into the models yielding a CT-based representation of the postoperative situation.

Evaluation of the image-free impingement detection technique

A detailed comparison between the intraoperatively acquired image-free ROM and the CT-based models was performed. Using the donor-specific three-dimensional bone model, ROM limitations were determined by an impingement detection technique, which was applied for different motion directions, that is, the leg was virtually moved until a collision between the three-dimensional objects (femoral vs pelvic components) occurred. Figure 3 shows this virtual assessment immediately before a bony impingement occurs in maximum external rotation. To establish a reference for leg movements, the coordinate systems of the pelvis and femur were aligned to define a neutral position (i.e. 0° flexion/extension, 0° abduction/adduction, and 0° internal/
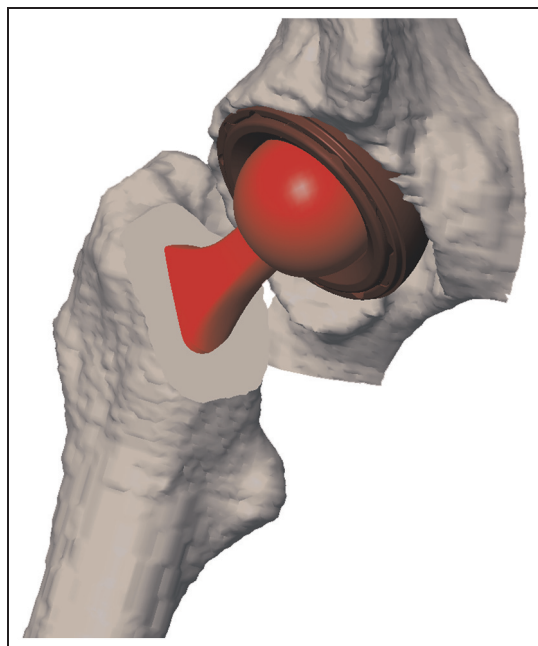
Figure 3. Impingement-free ROM is calculated based on three-dimensional models of the bony and prosthetic structures (intraoperative and CT-based models). ROM limitations were determined by virtually moving the leg until a collision between the 3D objects occurs. The maximum achievable ROM in the specified motion directions was determined. In this case, a bony impingement in external rotation at 0° flexion is shown.
ROM: range of motion; CT: computed tomography; 3D: three dimensional.

external rotation). The coordinate system of the pelvis was defined by the APP points. The connecting line between the ASIS points was used as a left–right direction, and the APP was used as a coronal plane. On the femoral side, the mechanical axis, that is, connecting line between the center of rotation and the center of the condyles, was used as the cranial–caudal direction. The plane spanned by the entry point of the proximal shaft, center of the condyles, and center of the ankle was used to define the rotational alignment of the coordinate system. This plane was required to be perpendicular to the coronal plane. Based upon these coordinate systems, the motion directions were defined according to the recommendations of the International Society of Biomechanics (ISB).[14] For each case and motion direction (flexion/extension, abduction/adduction, and internal/external rotation at 0° and 90° flexion), the achieved absolute ROM, that is, maximum ROM until a collision occurred, was determined using a collision detection technique similar to the approach presented by Jaramaz et al.[15] Then, the resulting ROM values between the navigation and CT model were compared in order to evaluate the accuracy and reliability of the image-free impingement detection method.

As a last step, it was analyzed whether the ROM assessments are accurate in everyday life situations, which are relevant for optimizing the cup position in THA. For this purpose, the results of the image-free

virtual and CT-based models were compared focusing on hip motion angles, which should be reached after THA for activities of daily living. This so-called intended range of motion (iROM) has been previously defined as hip flexion 130°, extension 40°, abduction 50°, adduction 50°, internal rotation at 0° flexion 80°, and external rotation at 0° flexion 40°. Following the clinical standard for intraoperative manual impingement testing, we expanded the definition for iROM with two additional directions of motion 30° internal rotation at 90° hip flexion and 30° external rotation at 90° hip flexion.[2,5,16–19] Additionally, a value for combined ROM was calculated as the average ROM for all eight motion directions.

Descriptive statistics, including means with 95% confidence intervals (CIs), standard deviation (SD) as well as minimum and maximum values, were calculated for the achieved ROM values regarding CT and intraoperative models. This was applied for the entire ensemble of ROM values as well as the subgroup of cases that showed ROM values below iROM for the particular motion directions. In particular, it was analyzed whether the deviation between CT and intraoperative models was below 5° for all these cases. Systematic deviation between the models was illustrated by Bland–Altman diagrams for the most important motion directions—flexion, abduction, internal rotation at 90° flexion, and external rotation at 0° flexion. Statistical analysis was performed using the R software package (version 2.13.0; R Foundation for Statistical Computing, Vienna, Austria).

Results

The overall results for the virtual impingement/ROM calculations are shown in Table 1. The mean values are shown graphically in Figure 4. Graphical representations of the deviations between CT-based and the intraoperative image-free virtual ROM analyses are illustrated in Figure 5(a) to (d) using Bland–Altman diagrams. For hip flexion, extension, and internal rotation, the 95% CIs lay within the range of −5° to 5°. For other motion directions, the 95% CIs exceeded this interval, when no further restrictions on the relevant ROM areas were applied. For several directions (i.e. hip abduction, internal rotation at 0° flexion, and external rotation at 0°/90° flexion), all ROM values were above iROM. Only for hip flexion, extension, adduction, and internal rotation at 90° flexion, some of the ROM values were within iROM. The statistics of the deviations in ROM values for all these cases are listed in Table 2. For the cases within this range, the deviation between the CT-based and the image-free ROM analyses was below 5° in all of these cases except for one adduction movement occurring at 37° of adduction as measured in the CT data set. In this particular case, an impingement occurred between the inferior rim of the acetabulum and the rim of the femoral resection plane.

Table 1. Descriptive statistics for the computer tomography (CT) and image-free hip range of motion (ROM)/impingement analyses including the difference between both measurement methods.

		CT-based ROM analysis (°)	ROM analysis intraoperative (image-free) models (°)	Difference between CT-based and image-free ROM (°)
Flexion	Mean ± SD	120.4 ± 10.3	121.1 ± 10.1	−0.7 ± 1.9
	95% Confidence interval	100.2 to 140.5	101.2 to 140.9	−4.4 to 2.9
	Range (minimum–maximum)	102 to 135	104 to 135	−4 to 3
Extension	Mean ± SD	67.6 ± 10.6	67.4 ± 10.9	0.3 ± 1.1
	95% Confidence interval	46.8 to 88.5	46.1 to 88.6	−1.8 to 2.4
	Range (minimum–maximum)	39 to 80	39 to 80	0 to 4
Abduction	Mean ± SD	63.8 ± 4.3	66.6 ± 3.1	−2.9 ± 3.2
	95% Confidence interval	55.4 to 72.1	60.6 to 72.7	−9.0 to 3.3
	Range (minimum–maximum)	57 to 72	61 to 72	−9 to 0
Adduction	Mean ± SD	52.9 ± 11.5	55.3 ± 9.6	−2.4 ± 6.0
	95% Confidence interval	30.5 to 75.4	36.5 to 74.1	−14.2 to 9.5
	Range (minimum–maximum)	37 to 64	41 to 64	−20 to 8
Internal rotation at 0° flexion	Mean ± SD	127.1 ± 12.5	127.7 ± 10.4	−0.6 ± 5.3
	95% Confidence interval	102.5 to 151.7	107.4 to 148.0	−11.0 to 9.7
	Range (minimum–maximum)	102 to 140	108 to 140	−8 to 12
External rotation at 0° flexion	Mean ± SD	59.6 ± 14.8	63.6 ± 17.6	−3.9 ± 6.7
	95% Confidence interval	30.6 to 88.7	29.0 to 98.1	−17.1 to 9.2
	Range (minimum–maximum)	40 to 93	43 to 97	−18 to 11
Internal rotation at 90° flexion	Mean ± SD	33.9 ± 14.0	34.1 ± 12.8	−0.3 ± 1.8
	95% Confidence interval	6.4 to 61.3	9.0 to 59.3	−3.8 to 3.3
	Range (minimum–maximum)	13 to 51	16 to 51	−4 to 4
External rotation at 90° flexion	Mean ± SD	107.4 ± 16.4	107.6 ± 18.4	−0.1 ± 4.9
	95% Confidence interval	75.2 to 139.6	71.5 to 143.7	−9.8 to 9.5
	Range (minimum–maximum)	77 to 140	69 to 140	−13 to 8

SD: standard deviation.

Table 2. Descriptive statistics for the difference between CT-based and image-free hip ROM analyses after reduction to the cases within iROM.

		Difference between CT-based and image-free ROM for cases within iROM (°)
Flexion	Number of values within iROM	14
	Mean ± SD	−0.8 ± 2.0
	95% Confidence interval	−4.7 to 3.2
	Range (minimum–maximum)	−4 to 3
Extension	Number of values within iROM	1
	Mean ± SD	0
	95% Confidence interval	—
	Range (minimum–maximum)	—
Adduction	Number of values within iROM	4
	Mean ± SD	−3.3 ± 2.2
	95% Confidence interval	−7.6 to 1.1
	Range (minimum–maximum)	−5 to 0
Internal rotation at 90° flexion	Number of values within iROM	6
	Mean ± SD	−1.2 ± 1.9
	95% Confidence interval	−5.0 to 2.6
	Range (minimum–maximum)	−4 to 1

SD: standard deviation; iROM: intended range of motion; CT: computed tomography.

Discussion

Our goal was to investigate the accuracy and assess the reliability of measuring bony and periprosthetic impingements on a virtual three-dimensional bone model with the help of image-free navigation technology. We hypothesized that this method achieves accurate results for ROM values that are crucial to obtain sufficient postoperative joint mobility for activities of daily living after THA (defined as iROM).

There are three limitations that need to be acknowledged and addressed regarding the present study. First, our analysis is limited by numbers. Second, the anatomic setting offers the chance for an idealized acquisition of landmarks. In a clinical situation, intraoperative palpation of defined bony landmarks by the surgeon
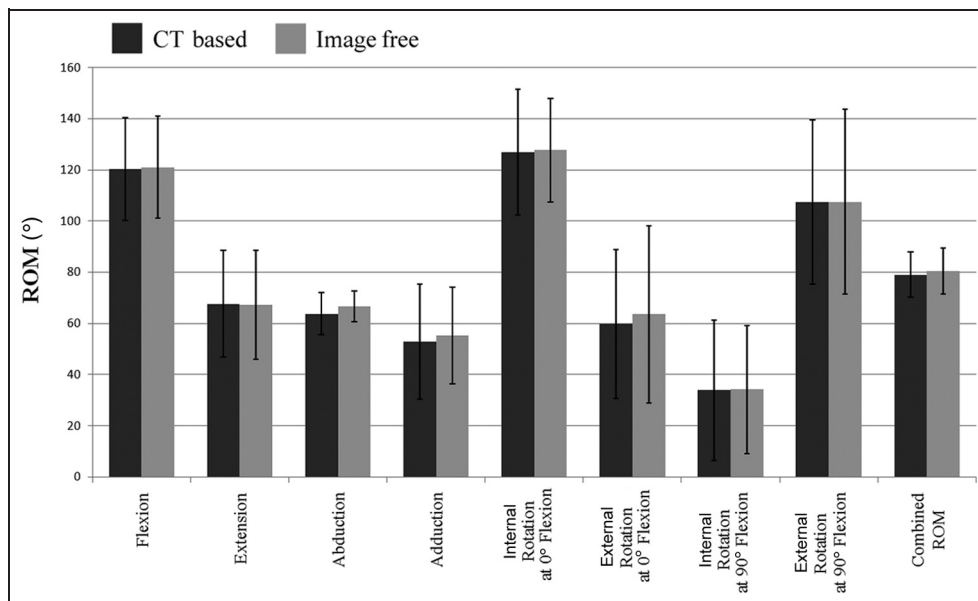
Figure 4. Overall comparison between the CT-based and image-free hip ROM analyses. Mean values are represented by column heights, 95% confidence intervals by error bars.
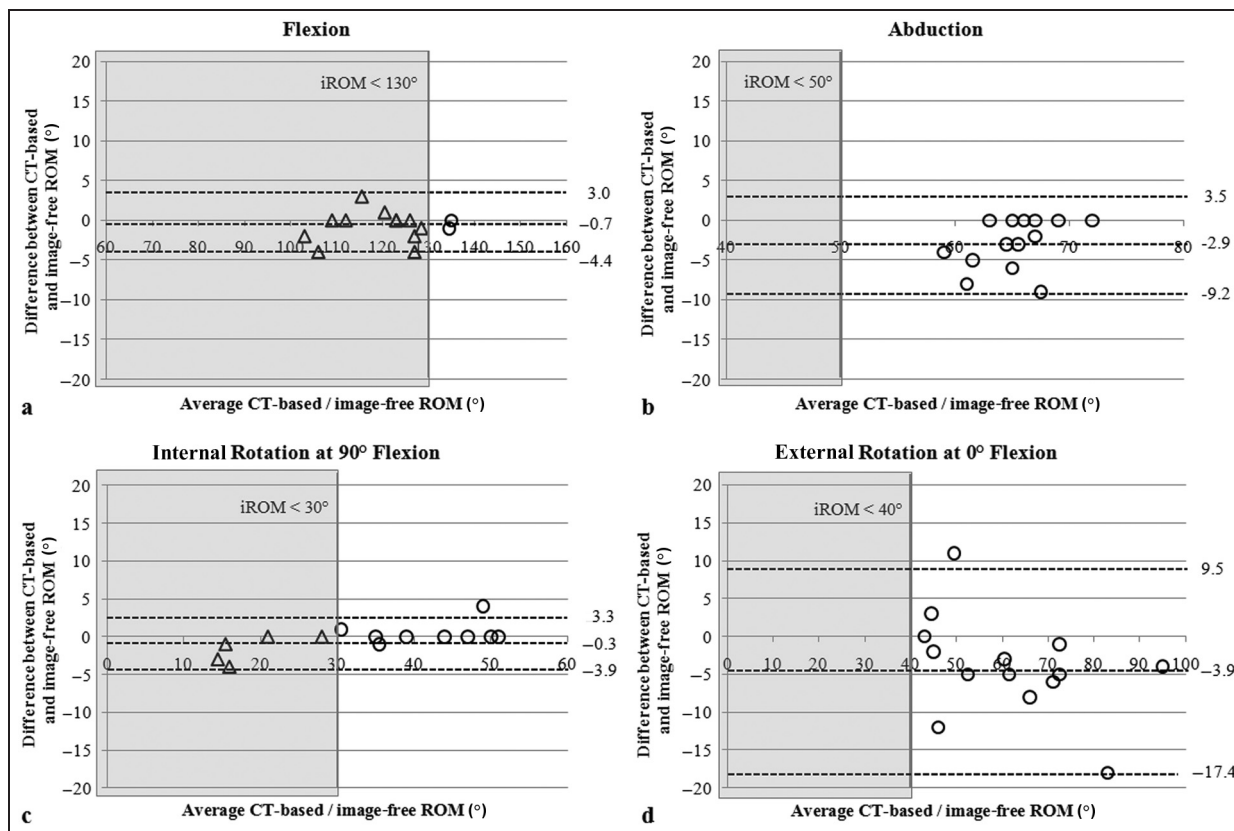CT: computed tomography; ROM: range of motion.

Figure 5. Bland–Altman diagrams depict the difference between the CT-based and image-free ROM analyses for (a) hip flexion, (b) hip abduction, (c) hip internal rotation at 90° flexion, and (d) hip external rotation at 0° flexion. The middle line represents the mean value of all differences between the pairs of measurements. The lines above and below it represent the 95% limits of expectable individual agreement (mean ± 1.96 standard deviations). ROM values within iROM are shown as triangles. Circles refer to ROM values outside iROM. The shaded area represents the region within iROM.
CT: computed tomography; ROM: range of motion; iROM: intended range of motion.

using a referenced pointer is a decisive process step during the computer navigation data entry process.[8] Since the system's calculations are solely based on the landmarks identified by the surgeon, inaccurate acquisition of these landmarks directly affects the calculation of the virtual joint model. Third, cadaveric tissue may not possess the same physical and mechanical properties as in vivo tissue. Using a minimally invasive hip approach and donors embalmed with Thiel's fixation method that allows a natural tissue feeling/joint movement, we tried to approximate the clinical situation.[9]

To the best of our knowledge, this is the first study to investigate the accuracy of this image-free navigation impingement detection technique during THA. Until now, virtual assessment of ROM was limited to a standardized prosthetic impingement analysis that cannot be transferred to the individual anatomy of the patient in detail.[16–20] Previously published CT-based analysis techniques implementing a detection of collisions between bony parts and/or prosthetic components have the need for an additional preoperative or intraoperative image acquisition and exposure to radiation.[21,22]

Our analysis revealed that bony and periprosthetic impingement can be generally detected by image-free navigation with an error range of below 5° for ROM values that are considered to be relevant for cup optimization in THA. There was only one case, reflecting an adduction movement, which was above the limit of 5° deviation. For the full ensemble of ROM values, most of the cases with high deviations between the CT-based and image-free approaches were related to impingements considerably outside iROM.[19] Such deviations are caused by an inaccurate reconstruction of the intraoperatively acquired bone model outside the periprosthetic area, since the navigation technique focuses on anatomical information around the acetabulum and femoral resection plane. For example, all measured ROM values (according to the image-free and CT-based analyses) for abduction, internal rotation at 0° flexion, and external rotation at 90° flexion were $> 15°$ outside iROM. Also for external rotation at 0° flexion, all impingements were found to be outside iROM.

Having demonstrated that bony and periprosthetic impingement can be accurately simulated during THA on a virtual three-dimensional bone model with the help of image-free navigation technology, our impingement detection method may now be established in clinical use. Previous studies have demonstrated that during the implantation process, depending on the anatomical shape of the femur, especially cementless stems virtually "find their way" to a rotational position, where the implant conforms best to the rigid shape of the native proximal femur canal. This results in a wide variability of stem antetorsion from 15° of retrotorsion to 45° of antetorsion.[23–25] In contrast, cup inclination and cup anteversion can be controlled to a certain extent by the surgeon during the reaming and implantation processes. In this context, different authors have proposed to consider cup and stem as components of a coupled biomechanical system, starting with the preparation of the femur ("femur first") and adjust the position of the cup in accordance with the femoral rotation.[8,16,25] Based upon the virtual three-dimensional bone model incorporating the registration of the patients' individual bony anatomy, stem position, and knowledge on the implants geometries, our image-free impingement detection technique has the potential to calculate a ROM optimized cup position with a reduced risk for impingement prior to the implantation of the cup intraoperatively.

Conflict of interest

The authors declare that they have no conflicts of interest.

References

1. Bozic KJ, Kurtz SM, Lau E, et al. The epidemiology of revision total hip arthroplasty in the United States. *J Bone Joint Surg Am* 2009; 91: 128–133.
2. Malik A, Maheshwari A and Dorr LD. Impingement with total hip replacement. *J Bone Joint Surg Am* 2007; 89: 1832–1842.
3. Brown T and Callaghan J. Impingement in total hip replacement: mechanisms and consequences. *Curr Orthop* 2008; 6: 376–391.
4. Padgett DE, Lipman J, Robie B, et al. Influence of total hip design on dislocation: a computer model and clinical analysis. *Clin Orthop Relat Res* 2006; 447: 48–52.
5. D'Lima DD, Urquhart AG, Buehler KO, et al. The effect of the orientation of the acetabular and femoral components on the range of motion of the hip at different head-neck ratios. *J Bone Joint Surg Am* 2000; 82: 315–321.
6. Woerner M, Weber M, Lechler P, et al. Minimally invasive surgery in total hip arthroplasty: surgical technique of the future? *Orthopade* 2011; 12: 1068–1074.
7. Kelley TC and Swank ML. Role of navigation in total hip arthroplasty. *J Bone Joint Surg Am* 2009; 91: 153–158.

8. Renkawitz T, Tingart M, Grifka J, et al. Computer-assisted total hip arthroplasty: coding the next generation of navigation systems for orthopedic surgery. *Expert Rev Med Devices* 2009; 5: 507–514.

9. Benkhadra M, Gérard J, Genelot D, et al. Is Thiel's embalming method widely known? A world survey about its use. *Surg Radiol Anat* 2011; 4: 359–363.

10. Besl P and McKay N. A method for registration of 3-D shapes. *IEEE T Pattern Anal* 1992; 14: 239–256.

11. Cootes TF, Taylor CJ, Cooper DH, et al. Active shape models—their training and application. *Comput Vis Image Und* 1995; 61: 38–59.

12. Szeliski R and Lavallée S. Matching 3-D anatomical surfaces with non-rigid deformations using octree-splines. *Int J Comput Vision* 1996; 2: 171–186.

13. Lewinnek GE, Lewis JL, Tarr R, et al. Dislocations after total hip-replacement arthroplasties. *J Bone Joint Surg Am* 1978; 60: 217–220.

14. Wu G Siegler S Allard P, et al. ISB recommendation on definitions of joint coordinate system of various joints for the reporting of human joint motion—part I: ankle, hip, and spine. International Society of Biomechanics. *J Biomech* 2002; 4: 543–548.

15. Jaramaz B, DiGioia AM, Blackwell M, et al. Computer assisted measurement of cup placement in total hip replacement. *Clin Orthop Relat Res* 1998; 354: 70–81.

16. Widmer KH and Zurfluh B. Compliant positioning of total hip components for optimal range of motion. *J Orthop Res* 2004; 22: 815–821.

17. Johnston RC and Smidt GL. Hip motion measurement for selected activities of daily living. *Clin Orthop Relat Res* 1970; 72: 205–215.

18. Jolles BM, Zangger P and Leyvraz PF. Factors predisposing to dislocation after primary total hip prosthesis. *J Arthroplasty* 2002; 17: 282–288.

19. Nadzadi ME, Pedersen DR, Yack HJ, et al. Kinematics, kinetics, and finite element analysis of commonplace maneuvers at risk for total hip dislocation. *J Biomech* 2003; 36: 577–591.

20. Yoshimine F and Ginbayashi KA. Mathematical formula to calculate the theoretical range of motion for total hip replacement. *J Biomech* 2002; 35: 989–993.

21. Tannast M, Kubiak-Langer M, Langlotz F, et al. Noninvasive three-dimensional assessment of femoroacetabular impingement. *J Orthop Res* 2007; 1: 122–131.

22. Kurtz WB, Ecker TM, Reichmann WM, et al. Factors affecting bony impingement in hip arthroplasty. *J Arthroplasty* 2010; 4: 624–634.

23. Wines AP and McNicol D. Computed tomography measurement of the accuracy of component version in total hip arthroplasty. *J Arthroplasty* 2006; 21: 696–701.

24. Sendtner E, Schuster T, Winkler R, et al. Stem torsion in total hip replacement. *Acta Orthop* 2010; 5: 579–582.

25. Dorr LD, Malik A, Dastane M, et al. Combined anteversion technique for total hip arthroplasty. *Clin Orthop Relat Res* 2009; 1: 119–127.